Study of Local and Nonlocal Poisson-Boltzmann Equations for Linear and Nonlinear Models with Spherical Symmetry

Hans W. Volkmer, Dexuan Xie*

Department of Mathematical Sciences, University of Wisconsin-Milwaukee, Milwaukee, WI, 53201-0413, USA

Abstract

In this paper, the local and nonlocal Poisson-Boltzmann equations are studied on their linear and nonlinear models with spherical symmetry. In particular, the exact solutions of the linear and nonlinear modes are obtained in either analytical expressions or simplified boundary value problems, whose solutions can be found easily via the Maple procedure dsolve for example. Numerical results confirm the derived solution properties, and show that the two new linear models proposed in this paper can have higher accuracy than the two conventional linear models in approximation to the local and nonlocal nonlinear models, respectively.

Key words: Poisson-Boltzmann equation, electrostatics, nonlocal dielectric, linear Poisson-Boltzmann models
2000 MSC: 35Q92, 92-08, 65L10, 92C40

1. Introduction

Prediction of electrostatics for protein in ionic solvent is a fundamental task in mathematical biology, biochemistry, biophysics, and biomedical science and engineering. The Poisson-Boltzmann equation (PBE) is one commonly-used dielectric continuum model for doing so, and has been applied to the study of biomolecular structure and function, catalytic activity, ligand association, and many bioengineering problems such as protein docking, ion channel modeling, and rational drug design [1, 2, 3, 4]. However, it simply treats the water solution as a uniform dielectric with a constant permittivity coefficient, ignoring the interactions or polarization correlation among the water molecules.

To remove such a drawback from PBE, a nonlocal modified PBE (NMPBE) model was developed recently in [5], along with a linear NMPBE model and efficient finite element solvers. The solution existence and uniqueness of NMPBE was also proved in [6]. Since NMPBE contains PBE as a special case, from the linear NMPBE models we can also obtain the well known linear PBE model. In [7], a novel linearization strategy was proposed to yield other linear PBE models. Following this strategy, another linear NMPBE model was reported and numerically solved in [8]. In this paper, we revisit this linearization strategy to produce two improved linear models for PBE and NMPBE, respectively. Due to simplicity and efficiency in implementation, these linear models can be valuable for applications that have sufficiently weak electrostatic fields. Hence, it is interesting for us to further explore and compare their qualities of approximations to the corresponding nonlinear models.

To do so, we study these linear and nonlinear models for a spherical solute region with one central charge only. In such a case, we can use the solution spherical symmetry to find the exact solutions of these models in either analytical expressions or simple boundary value problems. In this way, we can fairly compare these linear and nonlinear models. Furthermore, with the new analytical expressions and related boundary value problems, we did numerical tests on these linear and nonlinear models. Test results validate their derived solution properties, and display the solution differences. They also show that our new linear models can significantly improve the solution accuracy of the conventional linear models in comparison to the nonlinear PBE and NMPBE, respectively.

The remaining part of the paper is organized as follows. In Section 2, we review the NMPBE and PBE and their linear models. In Section 3, we study the solution properties of the linear and nonlinear PBE models with spherical

*Corresponding author. Email: dxie@uwm.edu.

symmetry. In Section 4, we study the solution properties of the linear and nonlinear NMPBE models with spherical symmetry. In Section 5, we present numerical results. The conclusions are made in Section 6.

2. Local and nonlocal Poisson-Boltzmann equations

In this section, we review the local and nonlocal Poisson-Boltzmann equations for a protein with n_p atoms in a symmetric 1:1 ionic solvent based on a decomposition of the whole space $\mathbb{R}^3$ in the form

$$\mathbb{R}^3 = D_p \cup D_s \cup \Gamma,$$

where D_p, D_s, and Γ denote a protein region, a solvent region, and an interface between D_p and D_s, respectively. In the continuum implicit solvent approach [9], D_p and D_s are treated as continuum dielectric media with two different dielectric constants ϵ_p and ϵ_s, respectively. A molecular structure of the protein is given with $\mathbf{r}_j$ and z_j denoting the position and charge number of atom j, respectively.

2.1. A nonlocal Poisson-Boltzmann equation

In [5, Eq. (21)], a nonlocal modified Poisson-Boltzmann equation (NMBE) is proposed as follows:

$$\begin{cases} -\epsilon_p \Delta u(\mathbf{r}) = \alpha \sum_{j=1}^{n_p} z_j \delta_{\mathbf{r}_j}, & \mathbf{r} \in D_p, \\ -\epsilon_\infty \Delta u(\mathbf{r}) + \frac{\epsilon_s - \epsilon_\infty}{\lambda^2}[u(\mathbf{r}) - (u * Q_\lambda)(\mathbf{r})] + \kappa^2 \sinh(u(\mathbf{r})) = 0, & \mathbf{r} \in D_s, \\ u(\mathbf{s}^-) = u(\mathbf{s}^+), \quad \epsilon_p \frac{\partial u(\mathbf{s}^-)}{\partial \mathbf{n}(\mathbf{s})} = \epsilon_\infty \frac{\partial u(\mathbf{s}^+)}{\partial \mathbf{n}(\mathbf{s})} + (\epsilon_s - \epsilon_\infty) \frac{\partial (u * Q_\lambda)(\mathbf{s})}{\partial \mathbf{n}(\mathbf{s})}, & \mathbf{s} \in \Gamma, \\ u(\mathbf{r}) \to 0 \qquad \text{as } |\mathbf{r}| \to \infty, \end{cases} \tag{2.1}$$

where u is a dimensionless electrostatic potential function, ϵ_∞ is another permittivity constant for D_p in the limit of high frequency [10], λ is a parameter for characterizing the polarization correlations of water molecules or the spacial-frequency dependence of a dielectric medium in a more general sense [11], $u * Q_\lambda$ denotes the convolution of u with a Yukawa-type kernel, $Q_\lambda(\mathbf{r}) = \frac{e^{-|\mathbf{r}|/\lambda}}{4\pi\lambda^2|\mathbf{r}|}$, [12, 13], $\mathbf{n}(\mathbf{s})$ denotes the unit outward normal vector of D_p, $\frac{\partial u(\mathbf{s})}{\partial \mathbf{n}(\mathbf{s})} = \nabla u(\mathbf{s}) \cdot \mathbf{n}(\mathbf{s})$, α and κ are given by

$$\alpha = \frac{10^{10} e_c^2}{\epsilon_0 k_B T}, \quad \kappa^2 = \frac{2 N_A e_c^2}{10^{17} \epsilon_0 k_B T} I_s,$$

and $\delta_{\mathbf{r}_j}$ denotes the Dirac-delta distribution at $\mathbf{r}_j$, which is defined by $\langle \delta_{\mathbf{r}_j}, v \rangle = v(\mathbf{r}_j)$ for any test function v. Here, e_c is the elementary charge, ϵ_0 is the permittivity of vacuum, k_B is the Boltzmann constant, I_s is an ionic strength in moles per liter, N_A is the Avogadro number, T is an absolute temperature, and length $|\mathbf{r}|$ is measured in angstroms (Å).

In the SI (Le Système International d'Unités) units, $e_c = 1.602176565 \times 10^{-19}$, $\epsilon_0 = 8.854187817 \times 10^{-12}$, $k_B = 1.380648813 \times 10^{-23}$, and $N_A = 6.0220450 \times 10^{23}$. With $T = 298.15$ and $I_s = 0.1$, we can get

$$\alpha \approx 7042.94, \quad \kappa^2 \approx 0.85, \tag{2.2}$$

and the solution u can be transformed to the electrostatic potential Φ in volts by the formula

$$\Phi(\mathbf{r}) = \frac{k_B T}{e_c} u(\mathbf{r}) \approx 0.02569\ u(\mathbf{r}) \text{ volts}, \quad \mathbf{r} \in \mathbb{R}^3.$$

One major difficulty in the analysis and numerical solution of NMPBE comes from the convolution term $u * Q_\lambda$. To avoid the difficulty, in [5], the convolution $u * Q_\lambda$ is treated as a unknown function so that NMPBE is reformulated

as a system with two unknown functions, u and w, as follows:

$$\begin{cases} -\epsilon_p \Delta u(\mathbf{r}) = \alpha \sum_{j=1}^{n_p} z_j \delta_{\mathbf{r}_j}, & \mathbf{r} \in D_p, \\ -\epsilon_\infty \Delta u(\mathbf{r}) + \frac{\epsilon_s - \epsilon_\infty}{\lambda^2}[u(\mathbf{r}) - w(\mathbf{r})] + \kappa^2 \sinh(u(\mathbf{r})) = 0, & \mathbf{r} \in D_s, \\ -\lambda^2 \Delta w(\mathbf{r}) + w(\mathbf{r}) - u(\mathbf{r}) = 0, & \mathbf{r} \in R^3, \\ u(\mathbf{s}^-) = u(\mathbf{s}^+), \quad \epsilon_p \frac{\partial u(\mathbf{s}^-)}{\partial \mathbf{n}(\mathbf{s})} = \epsilon_\infty \frac{\partial u(\mathbf{s}^+)}{\partial \mathbf{n}(\mathbf{s})} + (\epsilon_s - \epsilon_\infty) \frac{\partial w(\mathbf{s})}{\partial \mathbf{n}(\mathbf{s})}, & \mathbf{s} \in \Gamma, \\ u(\mathbf{r}) \to 0 \qquad \text{as } |\mathbf{r}| \to \infty. \end{cases} \tag{2.3}$$

2.2. Linear nonlocal Poisson-Boltzmann equations

A linearization strategy has been used in [7, 8] to construct linear models for PBE and NMPBE. In this strategy, an initial guess, u_0, to the solution u is supposed to give such that $|u - u_0| < 1$ in D_s. Thus, the approximations,

$$\sinh(u - u_0) \approx u - u_0, \quad \cosh(u - u_0) \approx 1,$$

can be used to linearize $\sinh(u)$ as shown below:

$$\sinh(u) = \sinh((u - u_0) + u_0) = \cosh(u - u_0)\sinh u_0 + \sinh(u - u_0)\cosh u_0 \approx \sinh u_0 + (u - u_0)\cosh u_0, \tag{2.4}$$

Applying (2.4) to the nonlinear NMPBE (2.3), we obtain a linear NMPBE model as follows:

$$\begin{cases} -\epsilon_p \Delta u(\mathbf{r}) = \alpha \sum_{j=1}^{n_p} z_j \delta_{\mathbf{r}_j}, & \mathbf{r} \in D_p, \\ -\epsilon_\infty \Delta u(\mathbf{r}) + \frac{\epsilon_s - \epsilon_\infty}{\lambda^2}[u(\mathbf{r}) - w(\mathbf{r})] + \kappa^2 \cosh(u_0) u(\mathbf{r}) = \kappa^2 [u_0 \cosh(u_0) - \sinh(u_0)], & \mathbf{r} \in D_s, \\ -\lambda^2 \Delta w(\mathbf{r}) + w(\mathbf{r}) - u(\mathbf{r}) = 0, & \mathbf{r} \in R^3, \\ u(\mathbf{s}^-) = u(\mathbf{s}^+), \quad \epsilon_p \frac{\partial u(\mathbf{s}^-)}{\partial \mathbf{n}(\mathbf{s})} = \epsilon_\infty \frac{\partial u(\mathbf{s}^+)}{\partial \mathbf{n}(\mathbf{s})} + (\epsilon_s - \epsilon_\infty) \frac{\partial w(\mathbf{s})}{\partial \mathbf{n}(\mathbf{s})}, & \mathbf{s} \in \Gamma, \\ u(\mathbf{r}) \to 0 \qquad \text{as } |\mathbf{r}| \to \infty. \end{cases} \tag{2.5}$$

Specifically, using $u_0 = 0$, we obtain the linear NMPBE model used in [5]:

$$\begin{cases} -\epsilon_p \Delta u(\mathbf{r}) = \alpha \sum_{j=1}^{n_p} z_j \delta_{\mathbf{r}_j}, & \mathbf{r} \in D_p, \\ -\epsilon_\infty \Delta u(\mathbf{r}) + \frac{\epsilon_s - \epsilon_\infty}{\lambda^2}[u(\mathbf{r}) - w(\mathbf{r})] + \kappa^2 u(\mathbf{r}) = 0, & \mathbf{r} \in D_s, \\ -\lambda^2 \Delta w(\mathbf{r}) + w(\mathbf{r}) - u(\mathbf{r}) = 0, & \mathbf{r} \in R^3, \\ u(\mathbf{s}^-) = u(\mathbf{s}^+), \quad \epsilon_p \frac{\partial u(\mathbf{s}^-)}{\partial \mathbf{n}(\mathbf{s})} = \epsilon_\infty \frac{\partial u(\mathbf{s}^+)}{\partial \mathbf{n}(\mathbf{s})} + (\epsilon_s - \epsilon_\infty) \frac{\partial w(\mathbf{s})}{\partial \mathbf{n}(\mathbf{s})}, & \mathbf{s} \in \Gamma, \\ u(\mathbf{r}) \to 0 \qquad \text{as } |\mathbf{r}| \to \infty, \end{cases} \tag{2.6}$$

which will be referred to as Linear nonlocal Poisson-Boltzmann equation 1 (LNPBE1).

When a solution, u_L, of LNPBE1 is known, it can be selected as u_0 to yield an improved linear model, called Linear nonlocal Poisson-Boltzmann equation 2 (LNPBE2). That is, LNPBE2 is defined by (2.5) with $u_0 = u_L$.

2.3. Poisson-Boltzmann equations

Obviously, setting $\epsilon_\infty = \epsilon_s$ immediately reduces the NMPBE model (2.1) to the Poisson-Boltzmann equation:

$$\begin{cases} -\epsilon_p \Delta u(\mathbf{r}) = \alpha \sum_{j=1}^{n_p} z_j \delta_{\mathbf{r}_j}, & \mathbf{r} \in D_p, \\ -\epsilon_s \Delta u(\mathbf{r}) + \kappa^2 \sinh(u(\mathbf{r})) = 0, & \mathbf{r} \in D_s, \\ u(\mathbf{s}^-) = u(\mathbf{s}^+), \quad \epsilon_p \frac{\partial u(\mathbf{s}^-)}{\partial \mathbf{n}(\mathbf{s})} = \epsilon_s \frac{\partial u(\mathbf{s}^+)}{\partial \mathbf{n}(\mathbf{s})}, & \mathbf{s} \in \Gamma, \\ u(\mathbf{r}) \to 0 \qquad \text{as } |\mathbf{r}| \to \infty. \end{cases} \tag{2.7}$$

Correspondingly, from LNPBE1 (2.6) there follows the traditional linear PBE:

$$\begin{cases} -\epsilon_p \Delta u(\mathbf{r}) = \alpha \sum\limits_{j=1}^{n_p} z_j \delta_{\mathbf{r}_j}, & \mathbf{r} \in D_p, \\ -\epsilon_s \Delta u(\mathbf{r}) + \kappa^2 u(\mathbf{r}) = 0, & \mathbf{r} \in D_s, \\ u(\mathbf{s}^-) = u(\mathbf{s}^+), \quad \epsilon_p \frac{\partial u(\mathbf{s}^-)}{\partial \mathbf{n}(\mathbf{s})} = \epsilon_s \frac{\partial u(\mathbf{s}^+)}{\partial \mathbf{n}(\mathbf{s})}, & \mathbf{s} \in \Gamma, \\ u(\mathbf{r}) \to 0 \qquad \text{as } |\mathbf{r}| \to \infty, \end{cases} \tag{2.8}$$

which will be denoted by LPBE1, while from LNPBE2 we can use a solution, u_L, of LPBE1 to obtain a new linear PBE model, denoted by LPBE2, as follows:

$$\begin{cases} -\epsilon_p \Delta u(\mathbf{r}) = \alpha \sum\limits_{j=1}^{n_p} z_j \delta_{\mathbf{r}_j}, & \mathbf{r} \in D_p, \\ -\epsilon_s \Delta u(\mathbf{r}) + \kappa^2 \cosh(u_L) u(\mathbf{r}) = \kappa^2 \left[u_L \cosh(u_L) - \sinh(u_L) \right], & \mathbf{r} \in D_s, \\ u(\mathbf{s}^-) = u(\mathbf{s}^+), \quad \epsilon_p \frac{\partial u(\mathbf{s}^-)}{\partial \mathbf{n}(\mathbf{s})} = \epsilon_s \frac{\partial u(\mathbf{s}^+)}{\partial \mathbf{n}(\mathbf{s})}, & \mathbf{s} \in \Gamma, \\ u(\mathbf{r}) \to 0 \qquad \text{as } |\mathbf{r}| \to \infty. \end{cases} \tag{2.9}$$

3. Analysis of local Poisson-Boltzmann models with spherical symmetry

In this section, we analyze the PBE models that are defined in (2.7), (2.8), and (2.9) on a spherical ball region $D_p = \{\mathbf{r} : |\mathbf{r}| < a\}$ with the radius $a > 0$ and one central charge ze_c (i.e., $n_p = 1$, $\mathbf{r}_1 = (0, 0, 0)$, and $z_1 = z$). In this case, we have that $\Gamma = \{\mathbf{r} : |\mathbf{r}| = a\}$, $D_s = \{\mathbf{r} : |\mathbf{r}| > a\}$, and the solutions u of these PBE models become radial functions (i.e., $u = u(r)$ with $r = |\mathbf{r}|$). Thus, the nonlinear PBE (2.7) can be reformulated as the nonlinear ordinary differential equation problem:

$$-\epsilon_p \left[\frac{d^2 u(r)}{dr^2} + \frac{2}{r} \frac{du(r)}{dr} \right] = \alpha z \delta_0, \qquad 0 < r < a, \tag{3.1}$$

$$-\epsilon_s \left[\frac{d^2 u(r)}{dr^2} + \frac{2}{r} \frac{du(r)}{dr} \right] + \kappa^2 \sinh u(r) = 0, \qquad r > a, \tag{3.2}$$

$$u(a^-) = u(a^+), \quad \epsilon_p \frac{du(a^-)}{dr} = \epsilon_s \frac{du(a^+)}{dr}, \qquad r = a, \tag{3.3}$$

$$u(r) \to 0 \qquad \text{as } r \to \infty. \tag{3.4}$$

Similarly, LPBE1 (2.8) can be reduced to the following linear ordinary differential equation problem:

$$-\epsilon_p \left[\frac{d^2 u_L(r)}{dr^2} + \frac{2}{r} \frac{du_L(r)}{dr} \right] = \alpha z \delta_0, \qquad 0 < r < a, \tag{3.5}$$

$$-\epsilon_s \left[\frac{d^2 u_L(r)}{dr^2} + \frac{2}{r} \frac{du_L(r)}{dr} \right] + \kappa^2 u_L(r) = 0, \qquad r > a, \tag{3.6}$$

$$u_L(a^-) = u_L(a^+), \quad \epsilon_p \frac{du_L(a^-)}{dr} = \epsilon_s \frac{du_L(a^+)}{dr}, \qquad r = a, \tag{3.7}$$

$$u_L(r) \to 0 \qquad \text{as } r \to \infty, \tag{3.8}$$

while LPBE2 (2.9) is simplified as the following linear ordinary differential equation problem:

$$-\epsilon_p\left[\frac{d^2u(r)}{dr^2}+\frac{2}{r}\frac{du(r)}{dr}\right]=\alpha z\delta_0, \qquad 0<r<a, \tag{3.9}$$

$$-\epsilon_s\left[\frac{d^2u(r)}{dr^2}+\frac{2}{r}\frac{du(r)}{dr}\right]+\kappa^2\cosh(u_L)u(r)=\kappa^2u_L\cosh(u_L)-\kappa^2\sinh(u_L), \qquad r>a, \tag{3.10}$$

$$u(a^-)=u(a^+), \quad \epsilon_p\frac{du(a^-)}{dr}=\epsilon_s\frac{du(a^+)}{dr}, \qquad r=a, \tag{3.11}$$

$$u(r)\to 0 \qquad \text{as } r\to\infty, \tag{3.12}$$

where u_L has been given as a solution of LPBE1.

We first look for the solution of the nonlinear PBE. To simplify notation we introduce three constants:

$$h=\kappa\epsilon_s^{-1/2}, \quad A_0=\frac{\alpha}{4\pi\epsilon_p}z, \quad S=-\frac{\epsilon_pA_0}{\epsilon_sa^2}. \tag{3.13}$$

Clearly, (3.1) yields that the solution $u(r)$ of the nonlinear PBE for $r<a$ has the expression

$$u(r)=\frac{A_0}{r}+B, \quad 0<r<a, \tag{3.14}$$

where B is a constant to be determined. The interface conditions of (3.3) are

$$\frac{A_0}{a}+B = u(a^+), \tag{3.15}$$

$$-\epsilon_p\frac{A_0}{a^2} = \epsilon_su'(a^+) \quad \text{or} \quad u'(a^+)=S. \tag{3.16}$$

Combining (3.2) with (3.16), we find that the solution $u(r)$ of the nonlinear PBE for $r>a$ satisfies the following nonlinear boundary value problem:

$$\begin{cases} -\dfrac{d^2u(r)}{dr^2}-\dfrac{2}{r}\dfrac{du(r)}{dr}+h^2\sinh u(r)=0, \quad r>a, \\ u'(a)=S, \quad \lim\limits_{r\to\infty}u(r)=0. \end{cases} \tag{3.17}$$

We next look for the solution of LPBE1. In this case, the solution $u_L(r)$ for $r>a$ is also determined by the above equations but with $\sinh u(r)$ replaced by $u(r)$. The solution u_L of this linear boundary value problem can be solved analytically in the expression:

$$u_L(r)=-\frac{Sa^2e^{ah}}{ah+1}\frac{e^{-hr}}{r}, \quad r>a. \tag{3.18}$$

For LPBE2 , we set $\psi=u-u_L$, where u_L is given. Rewriting (3.10), we can find that ψ is determined by the following linear boundary value problem

$$\begin{cases} -\frac{d^2\psi}{d^2r}-\frac{2}{r}\frac{d\psi}{dr}+h^2\cosh(u_L)\psi=\frac{d^2u_L}{d^2r}+\frac{2}{r}\frac{du_L}{dr}-h^2\sinh(u_L), \quad r>a, \\ \psi'(a)=S-u_L'(a), \quad \lim_{r\to\infty}\psi(r)=0. \end{cases} \tag{3.19}$$

Hence, when a solution ψ of the linear system (3.19) is given, we obtain the solution $u(r)$ of LPBE2 for $r>a$ by

$$u(r)=u_L(r)+\psi(r), \quad r>a.$$

Some solution properties of the linear and nonlinear PBE models are reported in Theorems 3.1 to 3.5.

From [14] we can get the following theorem.

Theorem 3.1. *The boundary value problem (3.17) has a unique solution, and the solution is positive, decreasing, and convex.*

Theorem 3.2. *Let ψ be a solution of the linear differential equation*

$$-\psi'' - \frac{2}{r}\psi' + g(r)\psi = h(r), \quad r \geq a > 0, \tag{3.20}$$

where $g(r), h(r)$ are continuous functions on $[a, \infty)$. If $g(r) > 0$ and $h(r) \geq 0$ for $r \geq a$, $\psi'(a) = 0$, and $\lim_{r\to\infty} \psi(r) = 0$, then $\psi(r) \geq 0$ for all $r \geq a$.

Proof. Suppose that $\psi(r) < 0$ for some $r \geq a$. There are two cases: If $\psi(a) \geq 0$, then ψ must have an absolute minimum at some $r_0 > a$ with $\psi(r_0) < 0$. Then $\psi'(r_0) = 0$ and $\psi''(r_0) \geq 0$. This contradicts (3.20) at $r = r_0$. If $\psi(a) < 0$ then (3.20) at $r = a$ yields $\psi''(a) < 0$. Therefore, again ψ has an absolute minimum at some $r_0 > a$, and we get a contradiction as before. □

In Theorem 3.3, we claim that all the linear models overestimate the true value of $u(r)$ for $r \geq a$.

Theorem 3.3. *If ψ is a solution of the linear boundary value problem (3.19), then $u(r) \leq u_L(r) + \psi(r)$ for all $r \geq a$.*

Proof. Set $\omega(r) = u_L(r) + \psi(r) - u(r)$. Then ω satisfies $\lim_{r\to\infty} \omega(r) = 0$, $\omega'(a) = 0$, and the differential equation

$$-\omega'' - \frac{2}{r}\omega' + h^2(\cosh u_L)\omega = h^2\left[\sinh u - \sinh u_L - (\cosh u_L)(u - u_L)\right].$$

The right-hand side is nonnegative because $u_L(r) \geq 0$ and $u(r) \geq 0$. Therefore, by Theorem 3.2, $\omega \geq 0$. □

In Theorem 3.4 we conclude that the values of $u_0 + \psi$ are smaller than u_0 when u_0 is given by u_L.

Theorem 3.4. *Let u_0 be a nonnegative function which satisfies the differential inequality*

$$-\frac{d^2u_0}{d^2r} - \frac{2}{r}\frac{du_0}{dr} + h^2 \sinh u_0 \geq 0, \quad r \geq a, \tag{3.21}$$

and the boundary conditions

$$u_0'(a) = S, \quad \lim_{r\to\infty} u_0(r) = 0.$$

If ψ is a solution of the following linear boundary value problem

$$\begin{cases} -\frac{d^2\psi}{d^2r} - \frac{2}{r}\frac{d\psi}{dr} + h^2\cosh(u_0)\psi = \frac{d^2u_0}{d^2r} + \frac{2}{r}\frac{du_0}{dr} - h^2\sinh(u_0), & r > a, \\ \psi'(a) = 0, \quad \lim_{r\to\infty} \psi(r) = 0, \end{cases} \tag{3.22}$$

then $\psi(r) \leq 0$ for all $r \geq a$. Thus, $u_0(r) + \psi(r) \leq u_0(r)$ for $r \geq a$.

If the inequality (3.21) is reversed, then $\psi(r) \geq 0$ so that $u_0(r) + \psi(r) \geq u_0(r)$ for $r \geq a$.

Proof. This follows immediately from Theorem 3.2. □

Theorem 3.5. *Let $u(r)$ be a solution to the boundary value problem (3.17). Then*

$$u(a) \leq 2\,\mathrm{arcsinh}\left(\frac{-S}{2h}\right), \tag{3.23}$$

and

$$u(r) \leq 2\ln\coth\left(\tfrac{1}{2}(r-a)h + \operatorname{arccoth} e^{\frac{1}{2}u(a)}\right) \quad \text{for } r \geq a. \tag{3.24}$$

Proof. We multiply (3.2) by $u'(r)$ and integrate between r and ∞. Then we obtain

$$\tfrac{1}{2}[u'(r)]^2 - \int_r^\infty \tfrac{2}{s}[u'(s)]^2\,ds + h^2[1 - \cosh u(r)] = 0.$$

Therefore,

$$\tfrac{1}{2}[u'(r)]^2 + h^2[1 - \cosh u(r)] \geq 0.$$

Since $u'(r) < 0$, this implies

$$-u'(r) \geq 2h \sinh\left(\frac{u(r)}{2}\right)$$

which gives (3.23) for $r = a$. Dividing by $\sinh(\frac{1}{2}u)$ and integrating from a to r we obtain

$$4 \operatorname{arccoth} e^{\frac{1}{2}u(r)} - 4 \operatorname{arccoth} e^{\frac{1}{2}u(a)} \geq 2h(r-a)$$

which gives (3.24). □

4. Analysis of nonlocal Poisson-Boltzmann models with spherical symmetry

In this section, we first look for the exact solution of the nonlinear NMPBE system (2.3) defined on a spherical ball region $D_p = \{\mathbf{r} : |\mathbf{r}| < a\}$ with the radius $a > 0$ and one central charge ze_c. Because of spherical symmetry, we can reduce it to a system of coupled nonlinear ordinary differential equations as follows:

$$-\epsilon_p \left[\frac{d^2u(r)}{dr^2} + \frac{2}{r}\frac{du(r)}{dr}\right] = \alpha z \delta_0, \qquad 0 < r < a, \tag{4.1}$$

$$-\frac{d^2u(r)}{d^2r} - \frac{2}{r}\frac{du(r)}{dr} + \frac{\epsilon_s - \epsilon_\infty}{\epsilon_\infty \lambda^2}[u(r) - w(r)] + \frac{\kappa^2}{\epsilon_\infty}\sinh u(r) = 0, \qquad r > a, \tag{4.2}$$

$$-\frac{d^2w(r)}{d^2r} - \frac{2}{r}\frac{dw(r)}{dr} + \frac{1}{\lambda^2}(w(r) - u(r)) = 0, \qquad r > 0, \tag{4.3}$$

$$u(a^-) = u(a^+), \quad \epsilon_p \frac{du(a^-)}{dr} = \epsilon_\infty \frac{du(a^+)}{dr} + (\epsilon_s - \epsilon_\infty)\frac{dw(a)}{dr}, \qquad r = a, \tag{4.4}$$

$$w(a^-) = w(a^+), \quad \frac{dw(a^-)}{dr} = \frac{dw(a^+)}{dr}, \qquad r = a, \tag{4.5}$$

$$u(r) \to 0 \qquad \text{as } r \to \infty. \tag{4.6}$$

Following what is done in [15], we can express the solution $(u(r), w(r))$ for $0 < r < a$ in the form:

$$u(r) = \frac{A_0}{r} + A_3, \quad 0 < r < a, \tag{4.7}$$

$$w(r) = \frac{A_4}{r}\sinh\frac{r}{\lambda} + \frac{A_0}{r}\left(1 - \cosh\frac{r}{\lambda}\right) + A_3, \quad 0 < r < a, \tag{4.8}$$

where A_3 and A_4 are constants which are yet unknown. Clearly, the solution $(u(r), w(r))$ for $r > a$ satisfies the differential equations (4.2), and (4.3). Using these equations and the interface conditions (4.4) and (4.5), we eliminate A_3 and A_4 to obtain that

$$\epsilon_\infty u'(a) + (\epsilon_s - \epsilon_\infty)w'(a) = -\frac{\epsilon_p A_0}{a^2}, \tag{4.9}$$

$$\left(a^2\cosh\frac{a}{\lambda} - a\lambda\sinh\frac{a}{\lambda}\right)(u(a) - w(a)) + a^2\lambda\sinh\left(\frac{a}{\lambda}\right)w'(a) = A_0\left(a - \lambda\sinh\frac{a}{\lambda}\right). \tag{4.10}$$

Thus, the differential equations (4.2) and (4.3) subject to the boundary conditions (4.9), (4.10), and

$$\lim_{r\to\infty} u(r) = 0, \quad \lim_{r\to\infty} w(r) = 0, \tag{4.11}$$

pose a nonlinear boundary value problem with solution $(u(r), w(r))$ for $r > a$.

Once we have (numerically) solved this problem we can determine A_3 and A_4 from (4.7), (4.8) and the interface conditions $u(a^-) = u(a^+)$, $w(a^-) = w(a^+)$. So we also know $(u(r), w(r))$ for $0 < r < a$.

We next determine the solution $(u_L(r), w_L(r))$ of the LNPBE1 (2.6). Clearly, the second and third equations of (2.6) can be simplified as

$$-\frac{d^2u_L}{d^2r} - \frac{2}{r}\frac{du_L}{dr} + \frac{\epsilon_s - \epsilon_\infty}{\epsilon_\infty \lambda^2}(u_L - w_L) + \frac{\kappa^2}{\epsilon_\infty}u_L = 0, \quad r > a, \tag{4.12}$$

and (4.3), respectively. System (4.12), (4.3) has solutions of the form

$$u_L(r) = c_1 \frac{e^{-\mu r}}{r}, \quad w_L(r) = c_2 \frac{e^{-\mu r}}{r},$$

where μ^2 and (c_1, c_2) are an eigenvalue and a corresponding eigenvector, respectively, of the matrix

$$M = \begin{bmatrix} \frac{\epsilon_s - \epsilon_\infty}{\epsilon_\infty \lambda^2} + \frac{\kappa^2}{\epsilon_\infty} & -\frac{\epsilon_s - \epsilon_\infty}{\epsilon_\infty \lambda^2} \\ -\frac{1}{\lambda^2} & \frac{1}{\lambda^2} \end{bmatrix}.$$

The above matrix M has two positive eigenvalues since $\kappa > 0$ and $0 < \epsilon_\infty < \epsilon_s$.

Let μ_1 and μ_2 be positive numbers such that μ_1^2 and μ_2^2 are the eigenvalues of M, respectively. Then the general solution of the system (4.12), (4.3) satisfying (4.11) is given by

$$u_L(r) = A_1(1 - \lambda^2\mu_1^2)\frac{e^{-\mu_1 r}}{r} + A_2(1 - \lambda^2\mu_2^2)\frac{e^{-\mu_2 r}}{r}, \tag{4.13}$$

$$w_L(r) = A_1 \frac{e^{-\mu_1 r}}{r} + A_2 \frac{e^{-\mu_2 r}}{r}, \tag{4.14}$$

where A_1, A_2, A_3 and A_4 are the parameters to be determined from the interface conditions (4.4) and (4.5). Alternatively, we can determine A_1, A_2 from the boundary conditions (4.9) and (4.10).

We now look for the solution of LNPBE2 . In LNPBE2 , for a given u_L, we set $\psi = u - u_L$, and define $R(r)$ by

$$R(r) = u_L''(r) + \frac{2}{r}u_L'(r) - \frac{\epsilon_s - \epsilon_\infty}{\epsilon_\infty \lambda^2} u_L(r) - \frac{\kappa^2}{\epsilon_\infty} \sinh u_L(r).$$

We find that ψ satisfies a linear ordinary differential equation system as follows:

$$\begin{cases} -\dfrac{d^2\psi}{d^2r} - \dfrac{2}{r}\dfrac{d\psi}{dr} + \dfrac{\epsilon_s - \epsilon_\infty}{\epsilon_\infty \lambda^2}(\psi - w) + \dfrac{\kappa^2}{\epsilon_\infty}\cosh(u_L)\psi = R(r), & r > a, \\ -\dfrac{d^2w}{d^2r} - \dfrac{2}{r}\dfrac{dw}{dr} + \dfrac{1}{\lambda^2}(w - \psi) = \dfrac{1}{\lambda^2}u_L(r), & r > a, \end{cases} \tag{4.15}$$

subject to the boundary conditions (4.9), (4.10), and (4.11) with u replaced by $u_L + \psi$. When ψ is found, we obtain the solution $u(r)$ of LNPBE2 for $r > a$ in the expression

$$u(r) = u_L(r) + \psi(r), \quad r > a.$$

5. Numerical results

In this section, we present numerical results to confirm our derived solution properties and show that our new linear models LPBE2 and LNPBE2 can significantly improve the accuracies of the conventional models LPBE1 and LNPBE1 in approximation to the nonlinear PBE and NMPBE models, respectively.

In all the numeidcal tests, we fixed these parameter values: $\epsilon_p = 2$, $\epsilon_s = 78.5$, $\lambda = 15$, and the values of α and κ of (2.2). The boundary condition $\lim_{r\to\infty} u(r) = 0$ was replaced by $u(b) = 0$ for $b = 100$, which was found by tests as a sufficiently large b. The solution $u_L(r)$ for $r > a$ of LPBE1 and LNPBE1 were computed by using the analytical formulas (3.14), (3.18) and (4.13). We then numerically solved the linear systems (3.19) and (4.15), respectively, to obtain the solutions of LPBE2 and LNPBE2. Because of our analytical work in Sections 3 and 4, the solutions of the nonlinear PBE and NMPBE models can now be easily found by solving the nonlinear boundary value problems — the equations of (3.17) for PBE and the equations of (4.2), (4.3), (4.9), (4.10), and (4.11) for NMPBE. In our tests, we wrote a Maple program and simply used the Maple procedure *dsolve* to solve all the related linear and nonlinear boundary value problems. The test results were reported in Tables 1 and 2 and Figures 1 and 2.

Table 1 compares the solution value $u(a)$ of the nonlinear PBE models with that of the two linear models LPBE1 and LPBE2 for $a = 1$ and the central charge number $z = 1, 2, 3$. From it we notice that the solution to the linear

Value of $u(a)$ with $a = 1$			
z	Nonlinear PBE	LPBE1	LPBE2
1	5.99838	6.46732	6.03484
2	8.18136	12.93464	11.93475
3	10.10087	19.40197	18.40197

Table 1: Comparison of the new linear model LPBE2 with the nonlinear PBE and conventional linear model LPBE1.

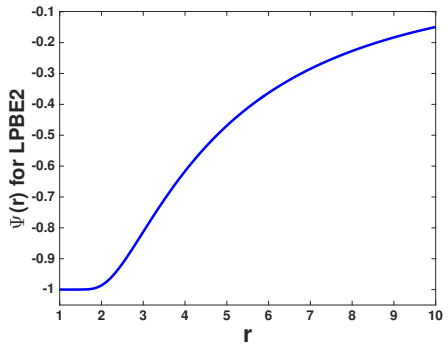

Figure 1: A function $\psi(r)$ of LPBE2 calculated by solving the boundary value problem (4.15) with $a = 1$ and $z = 3$.

problems overestimate the exact value of the nonlinear problem. These test results confirm Theorem 3.3, in which we claim that this is always true. We also notice that in the case $z = 1$, the solution to LPBE2 at $r = a$ is a much better approximation compared with the solution to LPBE1. It follows from Theorems 3.3, 3.4 that $\psi(r) < 0$ so we always get an improved approximation by LPBE2 compared with LPBE1.

From Table 1 we also see that when z gets larger, $u(a)$ and $u_L(a)$ increase; especially, $u_L(a)$ increases linearly with z. For example, the value of $u_L(a)$ for $z = 3$ is exactly three times the value of $u_L(a)$ for $z = 1$. It follows from Theorem 3.5 that $u(a)$ can have only logarithmic growth in z. This means that for large z the approximations to $u(a)$ are all very bad. We also notice that the approximation found by LPBE2 is almost exactly one unit better than $u_L(a)$ if $z \geq 2$. The reason for this is that $\sinh u_L(a)$ and $\cosh u_L(a)$ are very big numbers. In order to keep the balance in (3.19), $\psi(r)$ will be very close to -1 if r is close to a as shown in Figure 1.

Table 2 compares the interface values $u(a)$ of LNPBE1 with that of LNPBE2 for different selections of ϵ_∞. We

Value of $u(a)$ with $a = 1$ and $z = 1$			
ϵ_∞	NMPBE	LNPBE1	LNPBE2
70	6.45010	7.17630	6.56404
60	7.00994	8.25400	7.41450
50	7.58119	9.73790	8.76162
40	8.15392	11.91599	10.91635
30	8.74152	15.43830	14.43831
20	9.39691	22.16079	21.16079
10	10.29398	40.55436	39.55436

Table 2: Comparison of the new linear model LNPBE2 with the nonlinear NMPBE and conventional linear model LNPBE1.

notice that the value $u(a)$ of the nonlinear NMPBE increases when ϵ_∞ decreases. The same is true for the linear model LNPBE1 but $u(a)$ increases much faster than NMPBE. When ϵ_∞ is small, LNPBE1 is not a reasonable approximation for the nonlinear NMPBE anymore. From Table 2 it can also be seen that LNPBE2 is a better approximation to NMPBE than LNPBE1, in terms of $u(a)$, but it appears that the value $u(a)$ from LNPBE2 is almost exactly one unit less than that from LNPBE1. This can be explained from the form of equations (4.15). If ϵ_∞ is small, the potential function $u_L(r)$ produced from LNPBE1 is quite large for r close to a. Then $\sinh u_L(r)$ and $\cosh u_L(r)$ are huge numbers of almost the same size for r close to a. In order to balance these huge numbers, $\psi(r)$ $(= u - u_L)$ will be very close to -1 for r close to a. Since we only improve the result by one unit, it will take many iterations to get realistic approximations for the value $u(a)$ of the nonlinear NMPBE if ϵ_∞ is small. For example, if $\epsilon_\infty = 1.8$ (as chosen in [15]), then the linear model LNPBE1 has the value $u_L(a) \approx 161.50797$, which gives

$$\sinh u_L(a) \approx 6.9 \times 10^{69}.$$

These huge numbers cause problems in numerical calculation. This also illustrates that the linear model does not work any more as an approximation to the nonlinear model provided that $u_L(a)$ is too large (e.g., more than 10 as indicated in Table 2).

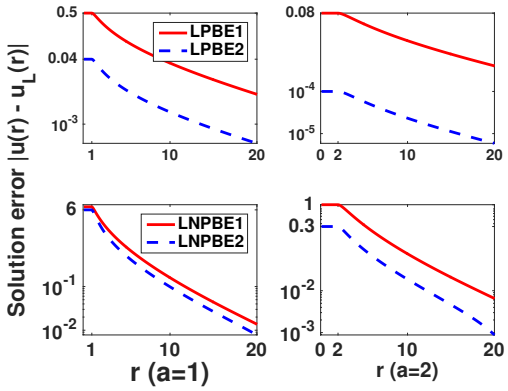

Figure 2: Comparison of new linear models LPBE2 and LNPBE2 with conventional linear models LPBE1 and LNPBE1 in solution error. Here, u denotes a solution of the nonlinear PBE/NMPBE, u_L denotes a solution of LPBE1, LPBE2, LNPBE1, or LNPBE2, and $z = 1$.

Figure 2 displays the solution errors between linear and nonlinear models as functions of r for $0 < r < 20$. Here, the error function was set as $|u(\mathbf{r}) - u_L(\mathbf{r})|$ with u_L and u denoting the solutions of the linear and nonlinear models, respectively. We repeated tests using $a = 1$ and $a = 2$ since the case of using $a = 1$ produced a stronger electric field than the case of using $a = 2$. These tests confirm that a linear model can be a good approximation to the corresponding nonlinear model when u is small enough, which leads to a weak electrostatic field. They also indicate that our new linear models LPBE2 and LNPBE2 have significantly improved the accuracy of the conventional linear models LPBE1 and LNPBE1 in approximation to the nonlinear PBE and NMPBE models.

6. Conclusions

In our model study we note that the approximations to the solution $u(r)$ of the nonlinear model for $r > a$ obtained by the linear models overestimate the true value of $u(r)$. If $u(a)$ is not too large (say $u(a) < 8$) or an electrostatic field is weak (e.g. the case of a solute ball with radius $a = 1$ and central charge $z = 1$), the linear models give us reasonably good approximations of $u(r)$. In particular, the new linear models LPBE2 and LNPBE2 give better approximations than the conventional linear models LPBE1 and LNPBE1, respectively. Moreover, when the electrostatic field is weak enough (say $u(a) < 5$, or for a solute ball with radius $a = 2$ and central charge $z = 1$), the approximation by LPBE2 and LNPBE2 appear to be quite satisfactory. Hence, both LPBE2 and LNPBE2 can be useful in the prediction of electrostatics due to their efficiency and simplification in calculation. While these spherical test models are valuable for us to explore the major properties of the local and nonlocal Poisson-Boltzmann equations, in the future, we plan to further study them for the case of a spherical ball region containing multiple point charges. We then extend them as the test models that can reflect the effects of ion sizes in the calculation of electrostatics and ionic concentrations.

References

[1] N. Baker, Improving implicit solvent simulations: a Poisson-centric view, Curr. Opin. Struc. Biol. 15 (2005) 137–143.

[2] F. Fogolari, A. Brigo, H. Molinari, The Poisson-Boltzmann equation for biomolecular electrostatics: A tool for structural biology, J. Mol. Recognit. 15 (6) (2002) 377–392.

[3] B. Lu, Y. Zhou, M. Holst, J. McCammon, Recent progress in numerical methods for the Poisson-Boltzmann equation in biophysical applications, Commun. Comput. Phys. 3 (5) (2008) 973–1009.

[4] C. L. Vizcarra, S. L. Mayo, Electrostatics in computational protein design, Current Opinion in Chemical Biology 9 (2005) 622–626.

[5] D. Xie, Y. Jiang, A nonlocal modified Poisson-Boltzmann equation and finite element solver for computing electrostatics of biomolecules, Journal of Computational Physics 322 (2016) 1 – 20.

[6] L. R. Scott, D. Xie, Analysis of a nonlocal Poisson-Boltzmann equation, Technical Report TR-2016-01, University of Chicago (2016). It is downloadable at https://pdfs.semanticscholar.org/50fe/81fec75139966c69b5f01d483250b9099eef.pdf.

[7] J. Li, D. Xie, A new linear Poisson-Boltzmann equation and finite element solver by solution decomposition approach, Communications in Mathematical Sciences 13 (2) (2015) 315–325.

[8] Y. Jiang, Nonlocal Debye-Hückel equations and nonlocal linearized Poisson-Boltzmann equations for electrostatics of electrolytes, Ph.D. dissertation, The University of Wisconsin-Milwaukee, Milwaukee, Wisconsin (June 2016).

[9] B. Roux, T. Simonson, Implicit solvent models, Biophys. Chem. 78 (1999) 1–20.

[10] G. Wilson, R. Chan, D. Davidson, E. Whalley, Dielectric properties of ices II, III, V, and VI, J. Chem. Phys. 43 (1965) 2384–2391.

[11] H. Yada, M. Nagai, K. Tanaka, The intermolecular stretching vibration mode in water isotopes investigated with broadband terahertz time-domain spectroscopy, Chemical Physics Letters 473 (4-6) (2009) 279–283.

[12] A. Hildebrandt, R. Blossey, S. Rjasanow, O. Kohlbacher, H.-P. Lenhof, Novel formulation of nonlocal electrostatics, Phys. Rev. Lett. 93 (10) (2004) 108104.

[13] A. Kornyshev, A. Nitzan, Effect of overscreeming on the localization of hydrated electrons, Zeitschrift für Physikalische Chemie 215 (6) (2001) 701–715.

[14] T. Gronwall, On the existence and properties of the solutions of a certain differential equation of the second order, Annals of Mathematics (1926) 355–364.

[15] D. Xie, H. Volkmer, A modified nonlocal continuum electrostatic model for protein in water and its analytical solutions for ionic Born models, Commun. Comput. Phys. 13 (1) (2013) 174–194.